Moroccan Journal of Chemistry
ISSN: 2351-812X
http://revues.imist.ma/?journal=morjchem&page=login
Chourti & al. / Mor. J. Chem. 8 N°1 (2020) 304-317

Relationships between crystalline structure and dielectric properties in $Sr_2Sm_{(1-x)}Nd_xTi_2Nb_3O_{15}$ ceramics

K. Chourti[(a,b)]*, P. Marchet[(c)], Y. Elhafiane[(c)], A. Bendahhou[(a,b)], S. El barkany[(a,b)], M. Karroua[(a,b)], M. Abou-salama[(a,b)]

[(a)] *Multidisciplinary Faculty of Nador, Department of Chemistry, 60700 Nador, Mohammed First University, Oujda, Morocco.*
[(b)] *Laboratory of Physical Chemistry of the Natural Resources and Environement (LACPRENE), Faculty of sciences, Mohammed First University, Oujda, Morocco.*
[(c)] *IRCER UMR7315, CNRS University of Limoges, European Ceramics Centre, 12 rue Atlantis, 87068 Limoges Cedex, France.*

* *Corresponding author:* chokarim@gmail.com
Received 20 Nov 2019, Revised 23 Feb 2020, Accepted 28 Feb 2020.

Abstract

In this study, tungsten-bronze type materials of $Sr_2Sm_{(1-x)}Nd_xTi_2Nb_3O_{15}$ composition (x=0; 0,25; 0,5; 0,75 and 1) were elaborated by classical solid-state reaction. The structural characterization demonstrate that these compounds present tetragonal symmetry, using two space groups P4bm (N°100) and P4/mbm (N°127) respectively. The lattice parameters are a=b≈12,2Å; c≈3,8Å; V≈579,0Å^3 and Z=2. In this compounds, Ti and Nb cations show obvious off-center displacements along the c axis in both the Ti/Nb(1)O_6 and the Ti/Nb(2)O_6 octahedra. Besides, the unequal Ti/Nb(2)–O bonds length in the equatorial plane of Ti/Nb(2)O_6 octahedra indicates the displacement of the Ti/Nb(2) cations in the ab plane, and no displacement of the Ti/Nb(1) cations exists in the ab plane. The results show that this material has two types of octahedral, first octahedron with little deformation around the Ti1/Nb1 and the second octahedron are more distorted around the Ti2/Nb2. The measurements of permittivity and dielectric losses of the ceramic samples performed between 25°C and 700°C (100Hz to 1MHz), high dielectric constants (ε_r=127 ~ 194) and low dielectric losses (tan(δ) around 10^{-4} at 1MHz) were found. The maximum value of the dielectric constant is obtained for x=0 (ε_r=194). The Curie temperature Tc decreases from 332 to 246°C as a function of the substitution of the samarium by neodymium. Detailed microstructural analysis by scanning electron microscope (SEM) and (EDS) for this compounds are also investigated.

Keywords: Tetragonal tungsten bronze, crystalline structure, X-ray diffraction, dielectric properties.

1. Introduction

Interesting dielectric properties and for some of them ferroelectric/piezoelectric properties, the tetragonal tungsten bronze materials (TTB) are used for varied applications in the field of microelectronic and microelectromechanical devices, such as capacitors or actuators and they attracted an increasing scientific interest [1-8]. Most of the dielectric applications are based on three criteria: high relative permittivity (ε_r), low values of dielectric loss (tanδ), and a coefficient of temperature (τ_ε) which must be nearest as possible of 0ppm/°C. The TTB are used in microelectronic devices since they fulfil some of these criteria. The TTB structure consists mainly of a complex array of distorted BO_6 octahedra sharing corners in the three directions of the space, what lets appear three different types of interstices: square tunnels (A1), pentagonal tunnels (A2) and triangular tunnels (C) which allows a large chemical flexibility and generates a significant number of possible compositions [9]. The general formula of TTB is $(A1)_2(A2)_4(C)_4(B1)_2(B2)_8O_{30}$ [10-14]. In this formula, the (A1) and (A2) sites are occupied by large monovalent ions (Na^+, K^+…), divalent ions (Sr^{2+}, Ba^{2+}…) or trivalent ions (Sm^{3+}, Bi^{3+}…). The triangular channels (C) can only contain relatively small ions such as Li^+ and are often empty. The (B1) and (B2) octahedral sites contains small and highly charged ions such as Nb^{4+}or Ti^{4+} [13, 15, 16]. The dielectric ceramics of TTB-type belonging to the quaternary system $AO\text{-}Ln_2O_3\text{-}TiO_2\text{-}M_2O_5$ (A=Ba, Sr. Ln=Sm, Nd and M=Y, Nb), have already been studied by several authors [17-21]. Among these compositions, materials such as $Ba_3La_3Ti_5Ta_5O_{30}$; $Ba_4La_2Ti_4Ta_6O_{30}$; $Ba_5LaTi_3Ta_7O_{30}$; present a high dielectric constant (ε_r=127,7 – 148), low dielectric losses ($\tan(\delta)=10^{-4}$ – 10^{-3} at 1MHz), and a relatively high temperature coefficient (τ_ε=-728 to -1347 ppm/°C) [22]. The compounds $Ba_2NdTi_2Ta_3O_{15}$; $Ba_3Nd_3Ti_5Ta_5O_{30}$ and $Ba_5NdTi_3Ta_7O_{30}$ has also been prepared and present interesting relative permittivity (ε_r=103,1 – 171,7) [4]. Furthermore. H. ZHANG et al [23], evidenced for the niobates $Sr_4R_2Ti_4Nb_6O_{30}$ (R=Sm and Nd), i.e. $Sr_4Nd_2Ti_4Nb_6O_{30}$ (SNTN) and $Sr_4Sm_2Ti_4Nb_6O_{30}$ (SSTN). The Curie temperature of these compounds are 260 and 370°C for SNTN and SSTN, respectively. Other compositions such as $Sr_4La_2Ti_4M_6O_{30}$ (M=Nb, Ta) [24], $Sr_5RTi_3Nb_7O_{30}$ (R = Gd, Dy) [25], $Sr_5SmTi_3Nb_7O_{30}$ and $Sr_4Sm_2Ti_4Nb_6O_{30}$ [26] have also been evidenced. In particular, we have noticed that the structural study of $Sr_2LnTi_2Nb_3O_{15}$ compounds (Ln: rare earth) and their solid solutions has not been performed at the present time. Thus the aim of this work is to study the solid solution $Sr_2Sm_{(1-x)}Nd_xTi_2Nb_3O_{15}$ ($0 \leqslant x \leqslant 1$) in order to: (i) check for the occurrence of the $Sr_2SmTi_2Nb_3O_{15}$ and $Sr_2NdTi_2Nb_3O_{15}$ compounds, (ii) establish the structural evolution in the solid solution, (iii) to study their electrical properties and (iv) to establish relationships between the crystalline structure and the dielectric properties.

Abbreviation

TTB	Tetragonal Tungsten Bronze	SSTN	$Sr_2SmTi_2Nb_3O_{15}$
ε_r	Dielectric constant	SS75TN	$Sr_2Sm_{0.75}Nd_{0.25}Ti_2Nb_3O_{15}$
tan(δ)	Dielectric losses	SS50TN	$Sr_2Sm_{0.5}Nd_{0.5}Ti_2Nb_3O_{15}$
τ_ε	Coefficient of temperature	SS25TN	$Sr_2Sm_{0.25}Nd_{0.75}Ti_2Nb_3O_{15}$
ppm/°C	Parts Per Million per degree Celsius	SNTN	$Sr_2NdTi_2Nb_3O_{15}$
CN	Coordination Number		

2. Materials and methods

2.1Synthesis and sintering

The $Sr_2Sm_{(1-x)}Nd_xTi_2Nb_3O_{15}$ compositions $Sr_2SmTi_2Nb_3O_{15}$; $Sr_2Sm_{0.75}Nd_{0.25}Ti_2Nb_3O_{15}$; $Sr_2Sm_{0.5}Nd_{0.5}Ti_2Nb_3O_{15}$; $Sr_2Sm_{0.25}Nd_{0.75}Ti_2Nb_3O_{15}$ and $Sr_2NdTi_2Nb_3O_{15}$; were prepared by a conventional solid-state reaction method. The chemical reaction for the synthesis is:

$$2SrCO_3 + \frac{(1-x)}{2}Sm_2O_3 + \frac{x}{2}Nd_2O_3 + \frac{3}{2}Nb_2O_5 + 2TiO_2 \rightarrow Sr_2Sm_{(1-x)}Nd_xNb_3Ti_2O_{15} + 2CO_2$$

The starting materials were high purity $SrCO_3$ (99,95%, Aldrich), Nd_2O_3 (99,99%, Sigma-Aldrich), Sm_2O_3 (99,99%, Aldrich), TiO_2 (99,99%, Aldrich), and Nb_2O_5 (99,99%, Aldrich). Before use, Sm_2O_3 and Nd_2O_3 were at 800°C for 30 minutes in order to remove any water and carbon dioxide. The starting powders were weighed according to the ground in an agate mortar in order to homogenize the powder and to decrease the grain size. The mixtures were the calcined in alumina crucibles at 1350°C for 12 hours in air, with a heating and a cooling rate of 5°C/min.

After synthesis, the powders were ground and pressed at 98MPa in order to obtain some cylindrical pellets of 12mm in diameter and approximately 2mm in thickness, These disks were sintered at 1350°C and 1400°C in air for 2h (5°C/min) in order to obtain ceramics with relative density higher than 90%.

2.2X-ray diffraction (XRD)

The crystal structure and structural evolution was studied by powder X-Ray diffraction (XRD, Bruker D8) using Cu $K_{\alpha 1}$ radiation (λ=1,5406Å) at room temperature. The XRD patterns were recorded for $5° \leqslant 2\theta \leqslant 120°$ with a step width of 0,02°. The Fullprof [27] and Jana 2006 software [28] were used to perform Rietveld refinement of the XRD patterns [29].

2.3Dielectric measurements

Before dielectric characterization, the experimental density of the ceramic samples was determined by Archimedes′ method. For the dielectric measurements, the ceramic pellets were elctroded on both sides using silver paste paint which was fired in air at 700°C for 30min. The relative permittivity and dielectric losses tan(δ) were determined using an impedance analyzer (HP 4194A) in a broad frequency range (100Hz – 1MHz) and for various temperatures (20°C – 800°C), using a 5°C/min heating and cooling rate.

2.4Scanning Electron Microscopy SEM and EDX analysis

The microstructure of the ceramic samples was studied by SEM (SEM Stereoscan S260, Cambridge Instruments). Chemical analysis was also performed by Energy Dispersive X-Ray Spectroscopy (EDX) in order to check for the correct stoichiometry of the ceramic samples.

3. Results and discussion

3.1Considerations concerning the stability of the TTB structure

The stability of the TTB structure such as the solid solution $Sr_2Sm_{(1-x)}Nd_XTi_2Nb_3O_{15}$ is linked to the structural parameters. It must comply with conditions such as geometry, the electronegativity, electro neutrality.

3.1.1 Geometrical conditions

The tolerance factor (t_A) for TTB structure has been discussed by Wakiya et al [30].This parameter allows to estimate the stability of the crystal structure [31, 32] when the value of (t_A) is higher than 0,95; Thus, the value of t_A can be calculated for the two sites based on geometrical considerations by the following equations:

$$t_{A1} = \frac{r_{A1} + r_O}{\sqrt{2}(r_B + r_O)} \qquad (1)$$

$$t_{A2} = \frac{r_{A2} + r_O}{\sqrt{23 - 12\sqrt{3}}(r_B + r_O)} \qquad (2)$$

Where t_{A1} and t_{A2} represent the tolerance factor of (A1) and (A2) sites respectively, r_A, r_B and r_O are the ionic radii of the ions for (A) sites, (B) sites, and oxygen ion, respectively $r(Sr^{2+})$=1,44Å 12-CN; $r(Sm^{3+})$=1,24Å; 12-CN; $r(Nd^{3+})$=1,27Å; 12-CN; $r(Ti^{4+})$=0,605Å; 6-CN; $r(Nb^{5+})$=0,64Å; 6-CN given by Shannon and Prewitt [33]. The tolerance factor (t_A) for the TTB structure is calculated using a combination of t_{A1} and t_{A2}:

$$t_A = \frac{t_{A1} + 2t_{A2}}{3} \qquad (3)$$

The stable compounds of TTB structure have a tolerance factor of close to 1. In the case of the $Sr_2Sm_{(1-x)}Nd_xTi_2Nb_3O_{15}$ solid solution, the (t_A) values ranges from 0,9350 (x=0) to 0,9385 (x=1) indicating probably stable TTB structures (fig. 1).

*3.1.2 **Condition of electronegativity***

The electronegativity difference between A and B ions and oxygen ion is another important parameter for assessing the stability of the structure [31, 32]. The more important is this difference, the more stable is the structure. The relative stability can be estimated using the following equation based on electronegativities :

$$e = \frac{(\chi_A - \chi_O) + (\chi_B - \chi_O)}{2} \qquad (4)$$

Where (χ_A-χ_O) and (χ_B-χ_O) are the electronegativity difference between (A_O) and (B_O) respectively. In the case of the $Sr_2Sm_{(1-x)}Nd_XTi_2Nb_3O_{15}$ solid solution, the effect of electronegativities can be calculated by the following equation:

$$e = \frac{2(\chi_{Sr}-\chi_O) + (1-x)(\chi_{Sm}-\chi_O) + (x)(\chi_{Nd}-\chi_O) + 2(\chi_{Ti}-\chi_O) + 3(\chi_{Nb}-\chi_O)}{8} \qquad (5)$$

The electronegativity of the chemical being 0,95 for Sr; 1,17 for Sm; 1,14 for Nd; 1,54 for Ti; 1,6 for Nb and 3,44 for O [34]. The calculation presents an increase of the ″e″ factor and thus an increase of the stability of the structure with the increasing values of x (Fig. 1.).

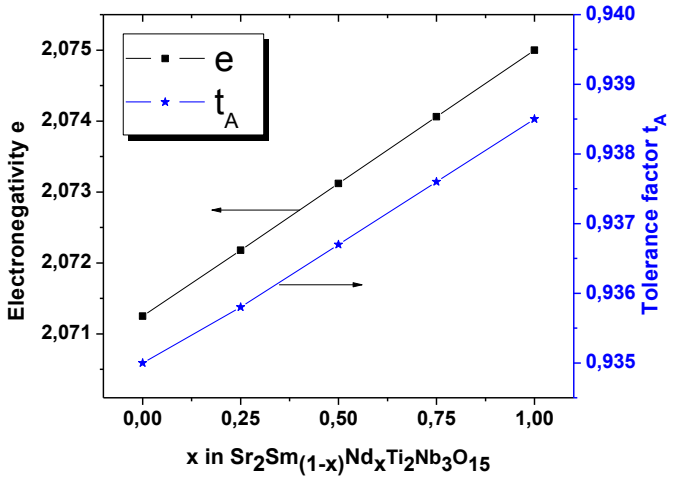

Fig. 1: *Variation of the electronegativity criteria (e) and tolerance factor (t_A) for the $Sr_2Sm_{(1-x)}Nd_xTi_2Nb_3O_{15}$ solid solution.*

3.2Structural study by X-ray diffraction

The XRD patterns for $Sr_2Sm_{(1-x)}Nd_xTi_2Nb_3O_{15}$ powders (x=0; 0,25; 0,5; 0,75 and 1) are represented fig.3. All of them are indexed as tetragonal tungsten bronze structure, unit cell a=b=12,22476 Å and c=3,85Å. Refinement of XRD data was carried out using the basic TTB structure [35] and [36] as a starting models with the two space groups, P4bm and

P4/mbm respectively. The final differences and profile fits are shown in Fig. 2. Nearly all peaks are indexed, with the exception of one very weak peak low intensity. Refinement in P4bm gave a much better fit than that in P4/mbm, with lower R factors (Table.1), and was adopted as the preferred model.

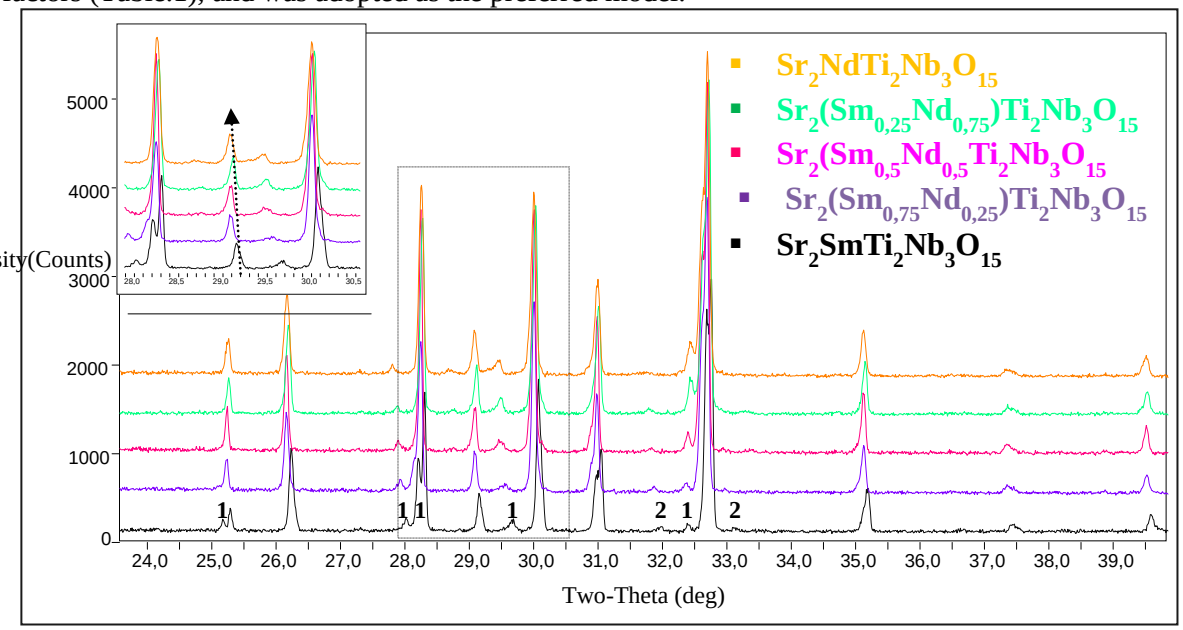

Fig. 2 : *XRD patterns of solid solution $Sr_2Sm_{(1-x)}Nd_xTi_2Nb_3O_{15}$ ($0 \leqslant x \leqslant 1$) at room temperature.* **1** *Minor amount of Nb_2O_5 and* **2** *$SmNbO_4$ secondary phases is detected.*

Rietveld refinement was performed for each pattern. As an example of such result, the final differences and profile fits for $Sr_2SmTi_2Nb_3O_{15}$ and $Sr_2NdTi_2Nb_3O_{15}$ are shown in Fig. 3.

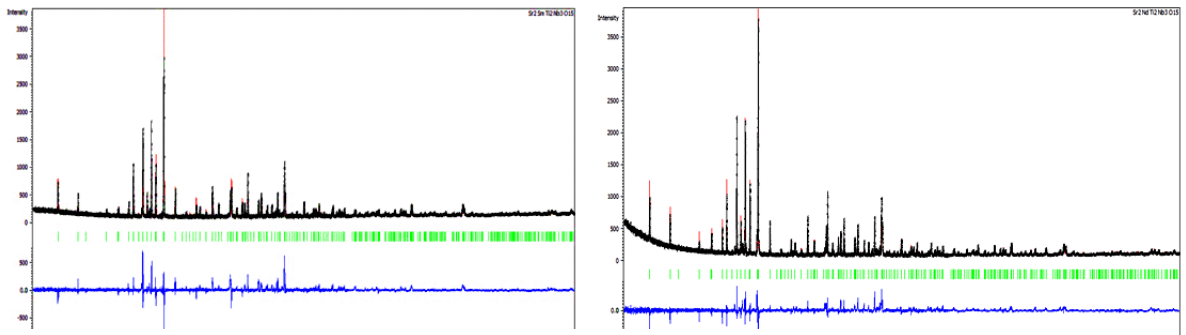

Fig. 3 : *Rietveld structural refinement result for $Sr_2SmTi_2Nb_3O_{15}$ (left) and $Sr_2NdTi_2Nb_3O_{15}$ (right).*

3.2.1 ***Evolution of lattice parameters***

The evolution of the ″a″ and ″c″ lattice parameters and unit cell volume ″V″ is represented Fig. 4. When substituting Nd for Sm, the ″c″ value increase, while the value of the ″a″ lattice parameter increase together with the lattice volume ″V″. This increase is logical since the ionic radius of neodymium (R_{Nd3+}=1,27Å) is higher than the one of samarium ion (R_{Sm3+}=1,24Å).

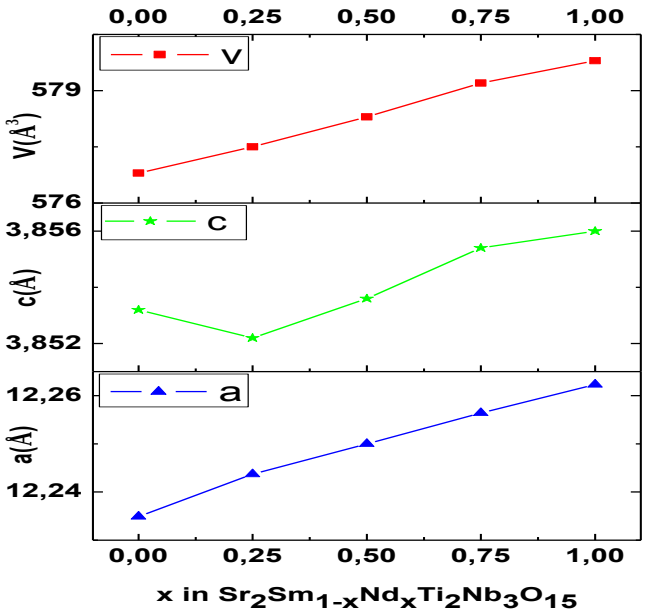

Fig. 4 : *Evolution of the lattice parameters and unit cell volume as a function of the composition for the solid solution* $Sr_2Sm_{(1-x)}Nd_XTi_2Nb_3O_{15}$ *(0 ⩽ x ⩽ 1) at room temperature.*

3.2.2 ***Evolution of*** $\frac{c}{a}$ ***value and octahedra distorsion***

According to R.J. Xie and al [37], the calculation of value of the tetragonal distortion $\frac{c}{a}$ allows to check if the octahedra undergo a distortion or not. Indeed when the value of $\frac{c}{a}\sqrt{10}$ is lower than 1, there is a distortion of the BO_6 octahedra. On the contrary, when this value is equal to 1, there is no distortion. For the $Sr_2Sm_{(1-x)}Nd_XTi_2Nb_3O_{15}$ solid solution, the calculated values are lower than unity (fig. 5) indicating a distortion of the BO_6 octahedra.

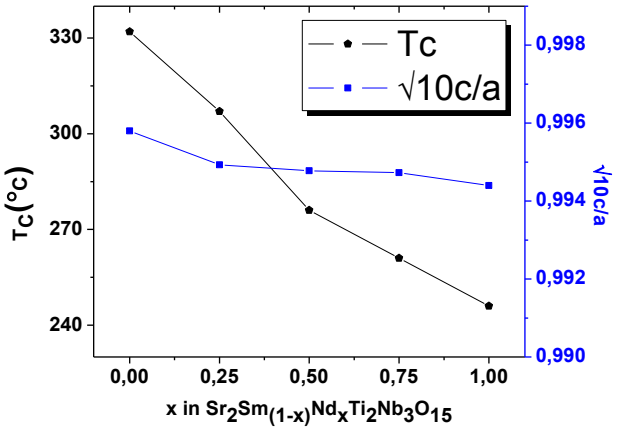

Fig. 5 : *Evolution of* $\frac{c}{a}\sqrt{10}$ *and Tc according to the composition for the solid solution* $Sr_2Sm_{(1-x)}Nd_XTi_2Nb_3O_{15}$ *(0⩽ x ⩽1)*

3.3Structural study by Rietveld refinement

The refinement has been led with the P4bm space group (no centrosymmetric). The values of the confidence factors, indicative of the quality of the refinement [38], are 8⩽ Rp ⩽11 and 12⩽ wRp ⩽15 (table. 1). These values are acceptable for a refinement performed by XRD on polycrystalline samples. The profile parameters, the atomic positions and the isotropic atomic displacement parameters of the atoms were also refined. The results as a function of

composition are given table. 2. The sites square (A1) (the perovskite site) are occupied by the cations of neodymium. When x increases, the (A2) sites are filled with strontium at the same time, and the atoms of titan and niobium in sites octahedral, the (C) sites remain empty. Our samples perfectly index themselves in the quadratic system. Can the weak increase of the stitch parameters with x be explained by the weak difference of the rays of the two pressed Sm^{3+} and Nd^{2+} (Δr=0,03 Å).

Table. 1 : *Confidence factors of the Rietveld refinement for the compositions* $Sr_2Sm_{(1-x)}Nd_xTi_2Nb_3O_{15}$

	x=0	x=0,25	x=0,5	x=0,75	x=1
Rp	8,73	7,91	9,13	11,12	8,79
wRp	12,48	11,25	13,55	15,61	12,41
GOF	1,56	1,43	1,76	1,95	1,51

The atomic positions for the $Sr_2NdTi_2Nb_3O_{15}$ composition are listed in the picture 2

Table. 2 : *Refined structural parameters for* $Sr_2SmTi_2Nb_3O_{15}$ *and* $Sr_2NdTi_2Nb_3O_{15}$ *from x-ray powder diffraction data.*

Atom	Site	X	Y	z	Occ	U iso
			$Sr_2SmTi_2Nb_3O_{15}$		(x=0)	
Sr	4g	0,1703(3)	0,6703(3)	0,9658 (4)	1	0.0154(15)
Sm	2a	0	0	0,0134(0)	1	0.0043(9)
Ti1	8j	0	0,5	0,4644(2)	0,4	0,0013(18)
Nb1	8j	0	0,5	0,4644(2)	0,6	0,0013(18)
Ti2	2c	0,0772(3)	0,2150(3)	0,4834(2)	0,4	0,0055(8)
Nb2	2c	0,0772(3)	0,2150(3)	0,4834(2)	0,6	0,0055(8)
O1	8j	0	0,5	-0,002(2)	1	0.0090(12)
O2	2d	0,2792(14)	0,7792(14)	0,4368(3)	1	0,0250(7)
O3	4h	0,0678(19)	0,2207(18)	0,0188(3)	1	0.1200(11)
O4	8j	0,3374(13)	0,0332(13)	0,5378(2)	1	0.0230(7)
O5	8j	0,1402(14)	0,0636(17)	0,5248(2)	1	0.0770(10)
			$Sr_2NdTi_2Nb_3O_{15}$		(x=1)	
Sr	4g	0,1706(2)	0,6706(2)	0,9640(4)	1	0,0355(14)
Nd	2a	0	0	-0,0004(0)	1	0,0045(8)
Ti1	8j	0	0,5	0,4640(2)	0,4	0,0175(15)
Nb1	8j	0	0,5	0,4671(2)	0,6	0,0175(15)
Ti2	2c	0,0758(2)	0,2148(2)	0,4861(2)	0,4	0,0055(7)
Nb2	2c	0,0758(2)	0,2148(2)	0,4861(2)	0,6	0,0055(7)
O1	8j	0	0,5	-0,0030(1)	1	0,121(18)
O2	2d	0,2766(13)	0,7766(13)	0,4340(2)	1	0,006(9)
O3	4h	0,0740(2)	0,2058(17)	0,0060(6)	1	0,134(11)
O4	8j	0,3428(10)	0,0052(9)	0,5350(2)	1	0,023(4)
O5	8j	0,1260(11)	0,0655(12)	0,560(13)	1	0,037(6)

The table gathers the main cation-anion distances resulting from the refinements for the different compositions studied.

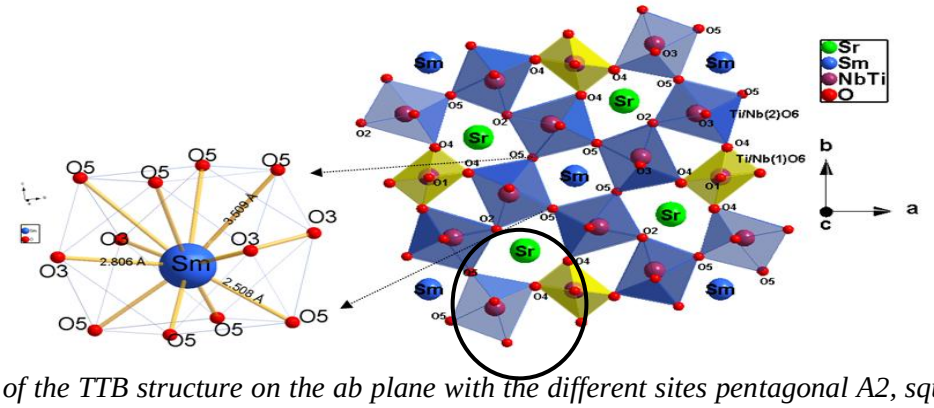

Fig. 6 : *Projection of the TTB structure on the ab plane with the different sites pentagonal A2, squares A1, and the C triangulars, for a niobate of* $Sr_2SmTi_2Nb_3O_{15}$ *formulation*

***Table**. 3 : Selected bond distances (Å) for* $Sr_2Nd_xSm_{1-x}Ti_2Nb_3O_{15}$

*"( ):Incertitude; * :Multiplicity; < >: Moyen value"*

Cation-O	SSTN	SS75NTN	SS50NTN	SS25NTN	SNTN
Sr-O(1)	2,9492(1)	2,96058(11)	2,96906(0)	2,89817(3)	2,938885(6)
Sr-O(3)	3,2099(2)*2	3,19995(16)*2	3,04921(0)*2	2,96087(4)*2	3,17689(7)
Sr-O(4)	2,3541(14)*2	2,86568(11)*2	2,82485(0)*2	2,76482(3)*2	2,86976(5)*2
Sr-O(4)′	2,7710(1)*2	2,64842(10)*2	2,70660(0)*2	2,64396(3)*2	2,75310(5)*2
Sr-O(5)	3,1572(1)*2	3,41044(11)*2	3,23269(0)*2	3,08327(3)*2	3,11988(5)*2
Sr-O(5)′	3,4232(2)*2	3,42079(11)*2	3,30566(0)*2	3,15973(3)*2	3,19559(5)*2
Sr-O(2)	2,6167(1)	2,51447(8)	2,50870(0)	2,51289(3)	2,72031(5)
Sr-O(2)′	2,7765(1)	2,71538(10)	2,60733(0)	2,61136(3)	2,62570 (4)
< Sr-O>	2,9072	2,9669	2,9005125	2,874375	2,92501
Nd-O(3)		2,69203(12)*4	2,7326	2,98483(4)*4	2,92301(7)*4
Sm-O(3)	2,8245(1)*4	2,69203(12)*4	2,73259(0)*4	2,98483(4)*4	
Nd-O(5)		2,53949(9)*4	2,63114(0)*4	2,93788(3)*4	2,751005(5)*4
Nd-O(5)′		2,62805(9)*4	2,78502(0)*4	2,79227(3)*4	2,89885(5)*4
Sm-O(5)	2,6632(1)*4	2,53949(9)*4	2,63114(0)*4	2,93788(3)*4	
Sm-O(5)′	2,7259(1)*4	2,62805(9)*4	2,78502(0)*4	2,79227(3)*4	
<Nd-O>		2,61985	2,66494	2,904993	2,85762
<Sm-O>	2,7378	2,61985	2,71625	2,904993	
Ti1/Nb1-O(1)	1,7901(15)	1,7055(1)	1,83442(6)	1,83619(3)	1,83610(5)
Ti1/Nb1-O(1)′	2,0629(17)	2,1469(1)	2,01878(6)	2,02095(3)	2,02126(5)
Ti1/Nb1-O(4)	2,0503(16)*4	1,9118(1)*4	1,94266(14)*4	1,68843(3)*4	1,85401(5)*4
<Ti1/Nb1-O>	1,9677	1,9214	1,9319	1,84850	1,90379
Ti2/Nb2-O(2)	1,9339(14)	1,99762(9)	2,00082(15)	2,04512(3)	1,90539(5)
Ti2/Nb2-O(3)	1,7952(15)	1,81734(10)	1,86058(15)	1,89549(3)	1,86777(5)
Ti2/Nb2-O(3)′	2,0674(17)	2,04107(11)	1,99902(3)	2,02979(3)	2,00546(5)
Ti2/Nb2-O(4)	2,0294(12)	1,91880(8)	1,94266(16)	2,12811(3)	1,8996(0)
Ti2/Nb2-O(5)	1,9559(13)	1,90468(9)	2,01487(3)	2,09194(3)	2,19195(5)
Ti2/Nb2-O(5)′	2,0102(15)	2,0249(0)	2,0478(4)	2,018(0)	2,0669(0)

< Ti2/Nb2-O>	1,9653	1,980401	2,005695	2,028045	2,020467

Substitution of samarium by neodymium in the square sites leads we have noticed: Two kinds of octahedral, the first octahedral Ti/Nb(1)O_6 is less distorted dTi/Nb(1)-O(4) the same distance for the five compounds equal to 1,8 Å and dTi/Nb(1)-O(1) less than dTi/Nb(1)-O(1)′, second octahedral Ti/Nb(2)O_6 more distorted, distances dTi/Nb(2)-O(2), dTi/Nb(2)-O(4) and dTi/Nb(2)-O(5) equals 2,0 Å. In this compounds studied (x = 0; 0,25; 0,5; 0,75 and 1) Ti and Nb cations show obvious off-center displacements along the c axis in both the Ti/Nb(1)O_6 and the Ti/Nb(2)O_6 octahedra. Besides, the unequal Ti/Nb(2)–O bonds length in the equatorial plane of Ti/Nb(2)O_6 octahedra indicates the displacement of the Ti/Nb(2) cations in the ab plane, and no displacement of the Ti/Nb(1) cations exists in the ab plane, which is obviously shown in the polyhedral representations along the c axis (Fig.7(a) and 7(b)). The insertion of neodymium into a square site leads to longer distances Ln-O, with dNd-O(3)=2,9230(7)Å and dNd-O(5)=2,7510(5)Å for the compound $Sr_2NdTi_2Nb_3O_{15}$; compared to the samarium compositions with dSm-O(3)=2,8245(1)Å and dSm-O(5)=2,6632(1)Å for $Sr_2SmTi_2Nb_3O_{15}$; in agreement with the ionic rays of these two lanthanides.

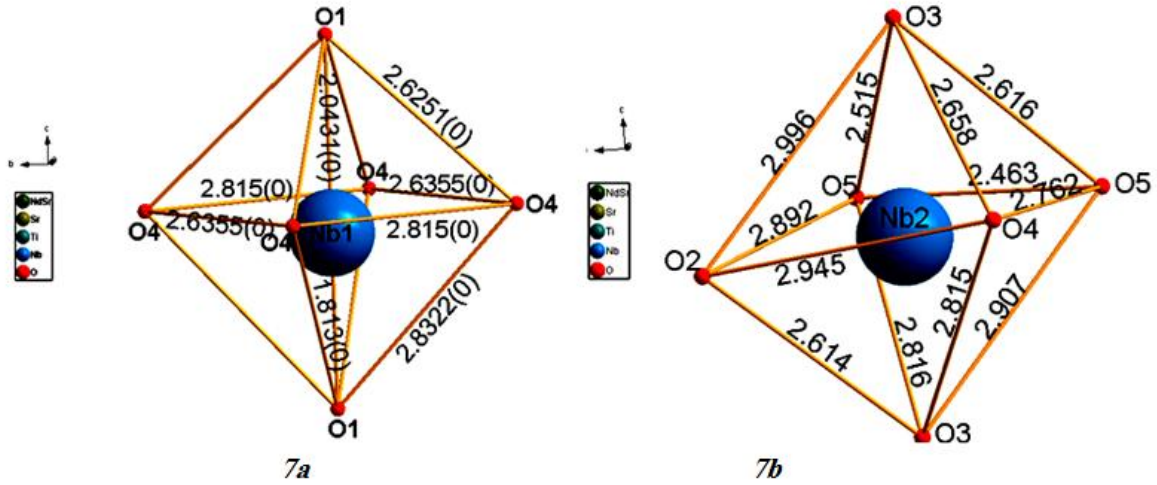

Fig. 7: *Polyhedral representations describing the distortions of the distortions of the two kinds of octahedral in $Sr_2Sm_{1-x}Nd_xTi_2Nb_3O_{15}$*

The density measurement is carried out by the method of Archimedes. The measured value is close to the theoretical value for all compounds. The difference can exist at the theoretical value of the solid solution, because for x>0, the density value is calculated by the values of the calculated mesh parameters.

Table. 4 *: Experimental and theoretical volume masses of $Sr_2Sm_{1-x}Nd_xTi_2Nb_3O_{15}$ compounds.*

Sample	Composition	ρcal(g/cm^3)
SSTN	$Sr_2SmNb_3Ti_2O_{15}$	5.382
SS75NTN	$Sr_2(Sm_{0,75}Nd_{0,25})Nb_3Ti_2O_{15}$	5.370
SS50NTN	$Sr_2(Sm_{0,5}Nd_{0,5})Nb_3Ti_2O_{15}$	5.357
SS25NTN	$Sr_2(Sm_{0,25}Nd_{0,75})Nb_3Ti_2O_{15}$	5.344
SNTN	$Sr_2NdNb_3Ti_2O_{15}$	5.324

3.4. Dielectric study

The Curie temperatures Tc, were determined by the variation of the real dielectric constant ε_r as a function of the temperature, at the different frequencies from 100Hz to 1MHz. Fig 8. Gives the variation of the dielectric constant ε_r

as a function of temperature. The ferroelectric-paraelectric phase transition temperature does not change as the frequency increases.

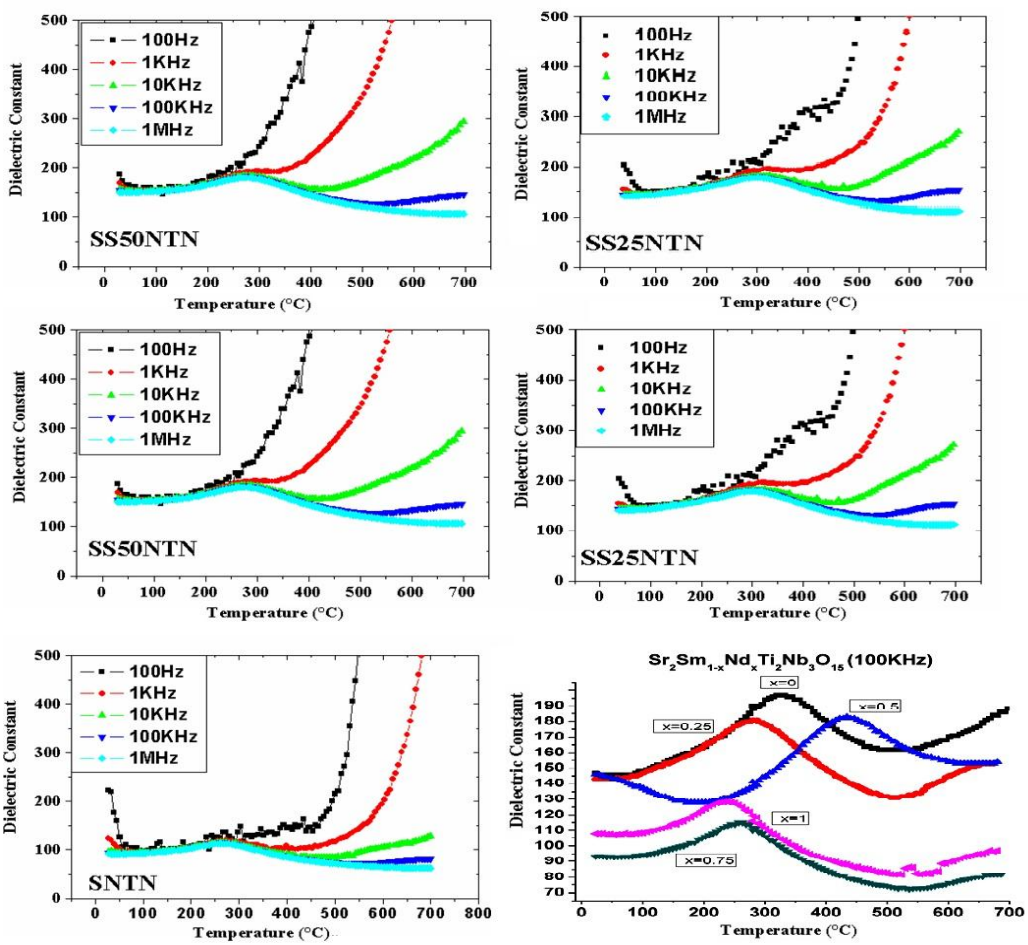

Fig. 8 : *Thermal evolution of the dielectric constant εr of SS(1-x)NxNT depending on the temperature at different frequencies: (a) x=0, (b) x=0.25, (c) x=0.5, (d) x=0.75, (e) x=1, and comparison of dielectric constant for x=0-1 at 100 kHz.*

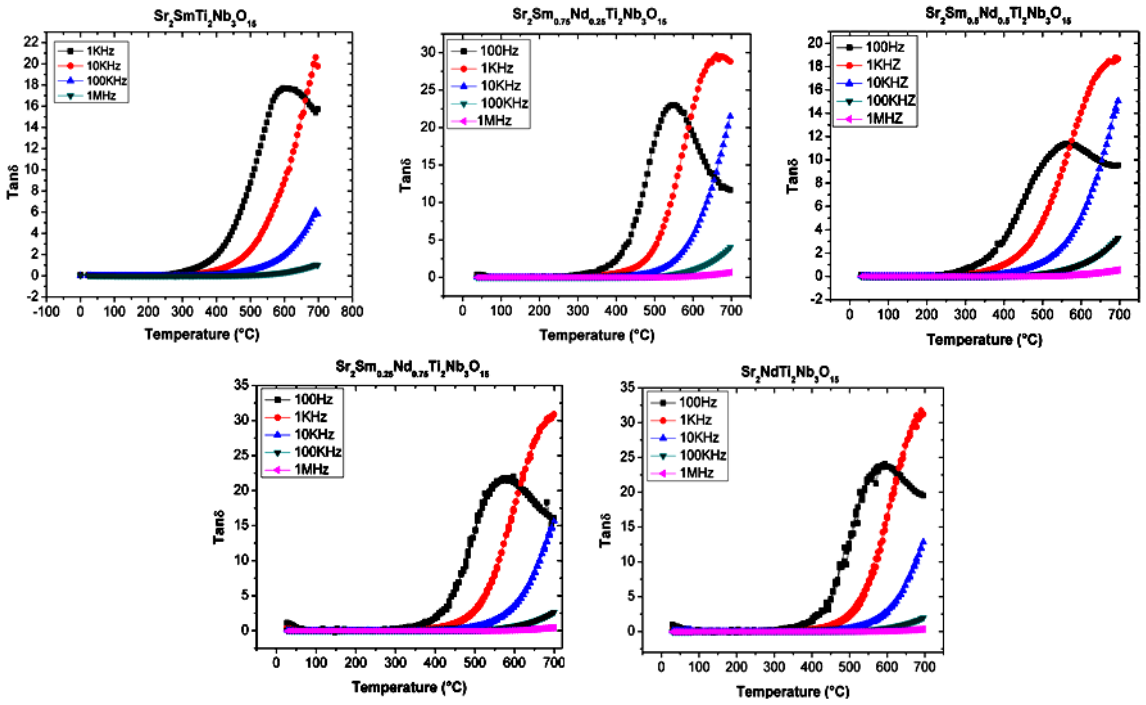

Fig. 9 : *Thermal evolution of the loss dielectric of* $Sr_2Sm_{1-x}Nd_xTi_2Nb_3O_{15}$

The phase transition temperature does not change when the frequency increases.

The dielectric constant decreases with increasing frequency for all compounds. The dielectric of ceramics SS(1-x)NxNT at room temperature are shown in fig 10. These ceramics have high dielectric constants ε_r varies between 194 (100% Sm) and 127 (100% Nd) and a low dielectric loss of the order of 10^{-4} at 1MHz.

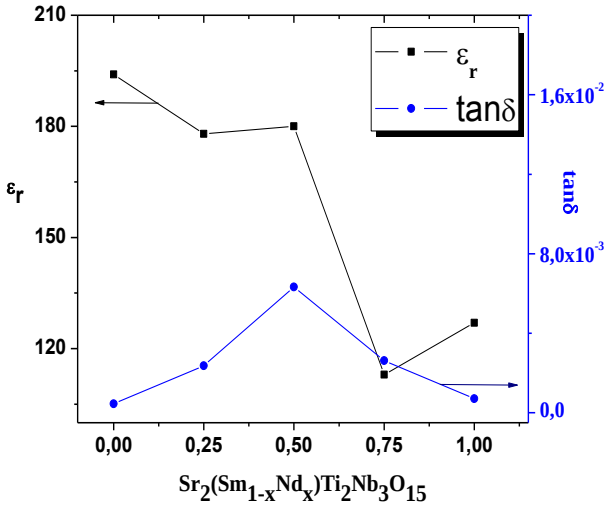

Fig. 1 *: Variation of* ε_r *and tan(δ) with composition x.*

The T_C value decreases as the size of the square-site cation increases that is when the samarium rate decreases. The Curie T_C temperature decreases from 332°C to 246°C (Fig.11). To verify the stoichiometry of our sintered pellets, we used X-ray energy dispersive spectroscopy (EDS) analysis. This technique has been used to ensure stoichiometry and to determine the possible presence of chemical elements in our ceramics. All the characteristic lines of our Sr, Sm, Nd, Nb, Ti and O chemical elements are present with varying rates depending on the chemical composition x.

The EDS spectra presented in fig. 11 allowed us to assert the purity of our samples and at the same time to continue the evolution of the neodymium rate which should normally increase from the composition SSTN to SNTN.

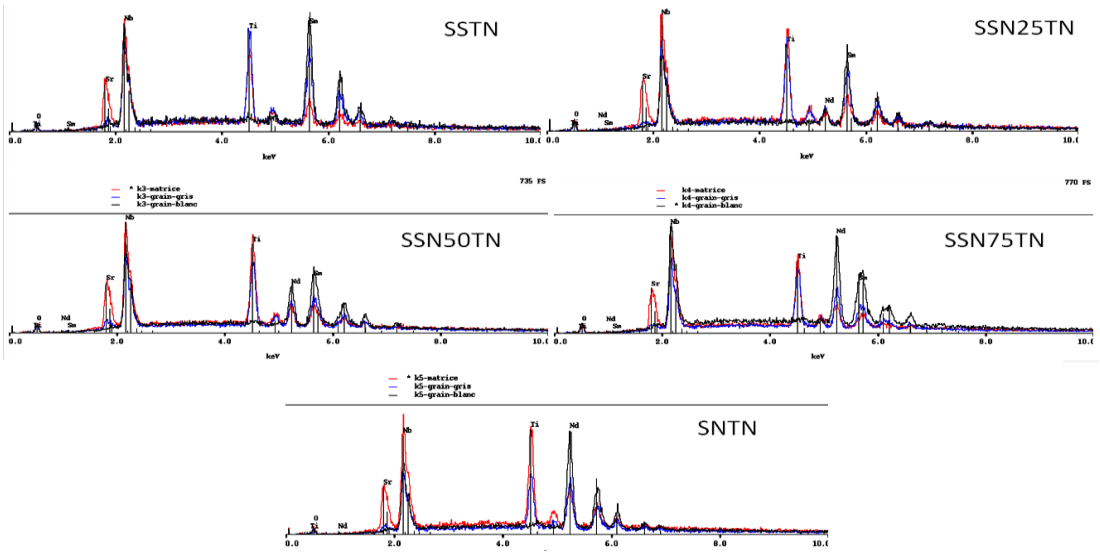

Fig. 2 : *Analysis by EDS spectroscopy of the solid solution* $Sr_2Sm_{(1-x)}Nd_xTi_2Nb_3O_{15}$

After the thermal treatment of the images on the surface of the pellets of our samples, were taken by scanning electron microscopy (SEM), fig. 12. The SEM images show grain sizes of less than 5µm with a good densification of the material which seems homogeneous.

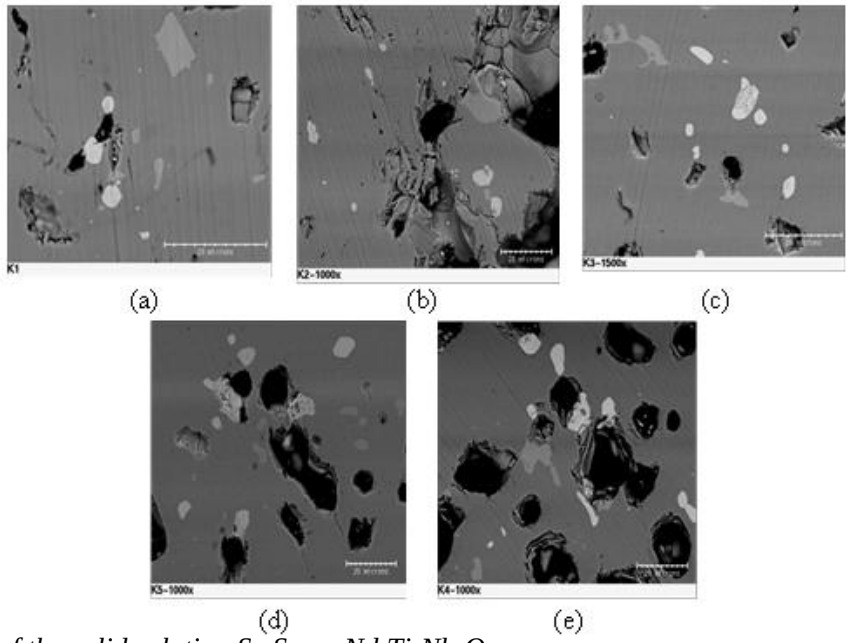

Fig. 12 : *SEM analysis of the solid solution $Sr_2Sm_{(1-x)}Nd_xTi_2Nb_3O_{15}$*
(a)=SSTN; (b)=SSN25TN; (c)=SSN50TN; (d)=SSN75TN and (e)=SNTN

4. Conclusion

This work allowed us to synthesize new compositions of general formula $Sr_2Sm_{1-x}Nd_xTi_2Nb_3O_{15;}$ x is between 0 and 1 belonging to the family of quadratic bronzes of tungsten, was evidenced by reaction to the state solid. A structural study by XRD on powder has shown that the crystalline structure must be described in the quadratic system, space group P4bm and the parameters a=b≈12,2Å; c≈3,8Å; V≈579,0$Å^3$; space group is P4bm. The dielectric measurements have shown that synthesized compounds have dielectric constants $\varepsilon_r \geqslant 127$ are ferroelectric and have a phase transition which depends on the composition x. The results showed that the phase transition temperature Tc decreases gradually from 332 to 246°C as the Sm^{3+} level decreases in the structure.

Reference

[1] P. Wise, I. Reaney, W. Lee, T. Price, D. Iddles, D. Cannell, Structure-microwave property relations of Ca and Sr titanates, Journal of the European Ceramic Society, 21 (2001) 2629-2632.

[2] L.A. Bendersky, J. Krajewski, R.J. Cava, Dielectric properties and microstructure of Ca5Nb2TiO12 and Ca5Ta2TiO12, Journal of the European Ceramic Society, 21 (2001) 2653-2658.

[3] H. Ohsato, Science of tungstenbronze-type like Ba6–3xR8+ 2xTi18O54 (R= rare earth) microwave dielectric solid solutions, Journal of the European Ceramic Society, 21 (2001) 2703-2711.

[4] X. Chen, J. Yang, J. Wang, LOW-LOSS DIELECTRIC CERAMICS WITH TUNGSTEN-BRONZE STRUCTURE IN BaO-Nd2O3-TiO 2-Ta 2 O 5 SYSTEM, Ceram. Trans, 100 (1999) 71-76.

[5] X. Chen, Z. Xu, J. Li, Dielectric ceramics in the BaO–Sm 2 O 3–TiO 2–Ta 2 O 5 quaternary system, Journal of Materials Research, 15 (2000) 125-129.

[6] M.T. Sebastian, H. Jantunen, Low loss dielectric materials for LTCC applications: a review, International Materials Reviews, 53 (2008) 57-90.
[7] L. Fang, L. Chen, H. Zhang, C. Diao, R. Yuan, Structural and dielectric properties of Ba5LnSn3Nb7O30 (Ln= La, Nd) ceramics, Materials Letters, 58 (2004) 2654-2657.
[8] X. Zheng, X. Chen, Temperature-Stable High-ε Dielectrics Ceramics Based on (1− x) Ba 5 NdTi 3 Ta 7 O 30/xBi 4 Ti 3 O 12, Journal of electroceramics, 10 (2003) 31-37.
[9] P. Labbe, Tungsten oxides, tungsten bronzes and tungsten bronze-type structures, in: Key Engineering Materials, Trans Tech Publ, 1992, pp. 293.
[10] A. Simon, J. Ravez, Solid-state chemistry and non-linear properties of tetragonal tungsten bronzes materials, Comptes Rendus Chimie, 9 (2006) 1268-1276.
[11] M. Prades, H. Beltrán, N. Masó, E. Cordoncillo, A.R. West, Phase transition hysteresis and anomalous Curie–Weiss behavior of ferroelectric tetragonal tungsten bronzes Ba 2 RETi 2 Nb 3 O 15: RE= Nd, Sm, Journal of Applied Physics, 104 (2008) 104118.
[12] D.C. Arnold, F.D. Morrison, B-cation effects in relaxor and ferroelectric tetragonal tungsten bronzes, Journal of Materials Chemistry, 19 (2009) 6485-6488.
[13] S. Lanfredi, D.H. Gênova, I.A. Brito, A.R. Lima, M.A. Nobre, Structural characterization and Curie temperature determination of a sodium strontium niobate ferroelectric nanostructured powder, Journal of Solid State Chemistry, 184 (2011) 990-1000.
[14] C. Dudhe, S. Nagdeote, C. Chaudhari, Ferroelectric Domains in Sr0. 5Ba0. 5Nb2O6 (SBN50) at Nanolevel, Ferroelectrics, 482 (2015) 104-112.
[15] J. Ravez, M. Dabadie, Influence de la substitution du fluor à l'oxygène sur les propriétés ferroélectriques de composés de structure" bronzes oxygénés de tungstène quadratiques", (1973).
[16] J. Ravez, A. Perron-Simon, P. Hagenmuller, Les phases de structure" bronzes de tungstèn quadratiques": règles cristallochimiques, relations entre propriétés ferroélectriques et distorsions structurales, (1976).
[17] M. Stennett, I. Reaney, G. Miles, D. Woodward, A. West, C. Kirk, I. Levin, Dielectric and structural studies of Ba 2 M Ti 2 Nb 3 O 15 (BM TNO 15, M= Bi 3+, La 3+, Nd 3+, Sm 3+, Gd 3+) tetragonal tungsten bronze-structured ceramics, Journal of Applied Physics, 101 (2007) 104114.
[18] X. Li Zhu, X. Ming Chen, Phase transition hysteresis of ferroelectric Sr5EuTi3Nb7O30 ceramics with tetragonal tungsten bronze structure, Journal of Applied Physics, 111 (2012) 044104.
[19] X. Chen, Y. Sun, X. Zheng, High permittivity and low loss dielectric ceramics in the BaO–La 2 O 3–TiO 2–Ta 2 O 5 system, Journal of the European Ceramic Society, 23 (2003) 1571-1575.
[20] M. Ranga Raju, R. Choudhary, H. Rukmini, Diffuse Phase Transition in Sr5RTi3Nb7O30 (R= La, Nd, Sm, Gd and Dy) Ferroelectric Ceramics, Ferroelectrics, 325 (2005) 25-32.
[21] L. Fang, H. Zhang, J. Yang, F. Meng, R. Yuan, Structural and dielectric properties of ferroelectric Sr 5 RTi 3 Nb 7 O 30 (R= Nd and Y) ceramics, Journal of materials science letters, 22 (2003) 1705-1707.
[22] X. Chen, Y. Sun, X. Zheng, High permittivity and low loss dielectric ceramics in the BaO–La2O3–TiO2–Ta2O5 system, Journal of the European Ceramic Society, 23 (2003) 1571-1575.
[23] H. Zhang, L. Fang, T. Huang, H. Liu, R. Yuan, R. Dronskowski, Structural and dielectric properties of ferroelectric Sr 4 R 2 Ti 4 Nb 6 O 30 (R= Sm and Nd) ceramics, Journal of materials science, 40 (2005) 529-531.
[24] L. Fang, H. Zhang, R. Yuan, R. Dronskowski, Characterization and dielectric properties of Sr 4 La 2 Ti 4 M 6 O 30 (M= Nb, Ta) ceramics, Journal of Materials Science: Materials in Electronics, 15 (2004) 699-701.
[25] M.R. Raju, R. Choudhary, Structural, dielectric and electrical properties of Sr5RTi3Nb7O30 (R= Gd and Dy)

ceramics, Materials Letters, 57 (2003) 2980-2987.
[26] Y. Sun, X. Chen, X. Zheng, Tungsten bronze type dielectrics in SrO-Sm 2 O 3-TiO 2-Nb 2 O 5 system and their dielectric anomaly, Journal of applied physics, 96 (2004) 7435-7439.
[27] J. Rodriguez-Carvajal, FULLPROF: a program for Rietveld refinement and pattern matching analysis, in: satellite meeting on powder diffraction of the XV congress of the IUCr, Toulouse, France:[sn], 1990.
[28] V. Petříček, M. Dušek, L. Palatinus, Crystallographic computing system JANA2006: general features, Zeitschrift für Kristallographie-Crystalline Materials, 229 (2014) 345-352.
[29] H. Rietveld, A profile refinement method for nuclear and magnetic structures, Journal of applied Crystallography, 2 (1969) 65-71.
[30] N. Wakiya, J.-K. Wang, A. Saiki, K. Shinozaki, N. Mizutani, Synthesis and dielectric properties of Ba 1− x R 2x/3 Nb 2 O 6 (R: rare earth) with tetragonal tungsten bronze structure, Journal of the European Ceramic Society, 19 (1999) 1071-1075.
[31] X. Zhu, M. Fu, M. Stennett, P. Vilarinho, I. Levin, C. Randall, J. Gardner, F. Morrison, I. Reaney, A crystal-chemical framework for relaxor versus normal ferroelectric behavior in tetragonal tungsten bronzes, Chemistry of Materials, 27 (2015) 3250-3261.
[32] X. Zheng, X. Chen, Dielectric ceramics with tungsten-bronze structure in the BaO–Nd2O3–TiO2–Nb2O5 system, Journal of materials research, 17 (2002) 1664-1670.
[33] R.T. Shannon, C.T. Prewitt, Effective ionic radii in oxides and fluorides, Acta Crystallographica Section B: Structural Crystallography and Crystal Chemistry, 25 (1969) 925-946.
[34] W.M. Haynes, CRC handbook of chemistry and physics, CRC press, 2014.
[35] X. Zhu, X. Chen, X. Liu, Y. Yuan, Dielectric characteristics and diffuse ferroelectric phase transition in Sr 4 La 2 Ti 4 Nb 6 O 30 tungsten bronze ceramics, Journal of materials research, 21 (2006) 1787-1792.
[36] V. Bovtun, S. Kamba, S. Veljko, D. Nuzhnyy, K. Knížek, M. Savinov, J. Petzelt, Relaxor-like behavior of lead-free Sr 2 LaTi 2 Nb 3 O 15 ceramics with tetragonal tungsten bronze structure, Journal of Applied Physics, 101 (2007) 054115.
[37] R.-J. Xie, Y. Akimune, Lead-free piezoelectric ceramics in the (1− x) Sr 2 NaNb 5 O 15–x Ca 2 NaNb 5 O 15 (0.05≤ x≤ 0.35) system, Journal of Materials Chemistry, 12 (2002) 3156-3161.
[38] R.J. Hill, R.X. Fischer, Profile agreement indices in Rietveld and pattern-fitting analysis, Journal of Applied Crystallography, 23 (1990) 462-468.